Szpak, S. and P.A. Mosier-Boss, *Nuclear and Thermal Events Associated with Pd + D Codeposition.* J. New Energy, 1996. **1**(3): p. 54.

NUCLEAR AND THERMAL EVENTS ASSOCIATED WITH Pd + D CODEPOSITION

S. Szpak and P.A. Mosier-Boss[1]

ABSTRACT

In the Pd+D codeposition process, palladium is electrodeposited in the presence of evolving deuterium. This process favors the initiation and propagation of nuclear and thermal events through a rapid absorption of deuterium to yield high D/Pd atomic ratios. This process results in the formation of non-equilibrium electrode structures that become the seat for localized gradients. Evidence for tritium production, X-ray emanation and generation of localized heat sources, with emphasis on experimental methodology, is provided. The active role of the electrode/electrolyte interphase in the development of these events is examined.

1.0 INTRODUCTION

The main obstacle in accepting that nuclear and thermal events can, and do, occur during electrochemical compression of the Pd/D system was, and still is, their poor reproducibility. The lack of sound theoretical guidance is the primary reason for this difficulty. An experimental approach to resolve this situation rests with the construction of the "performance envelope," *i.e.*, the listing of all factors contributing to the initiation and propagation of these events. In particular, one must consider changes that take place as the concentration of deuterons rises to be *ca* 100 molar with even higher concentration of electrons (*ca* 1000 molar) [l]. Consequently, in an attempt to construct the "performance envelope" one must examine the state of the Pd/D system as the D content increases, with emphasis on interfacial and transport phenomena.

1.1 Triggering conditions.

A review of published material indicates that the triggering conditions fall into three categories: (i) high D/Pd atomic ratio, with D/Pd > 0.85, (ii) metallurgical aspects of the electrode material, such as grain size, number and kind of defects, the presence of voids and fissures, *etc.*, and (iii) electrochemical aspects, *eg*, the structure of the electrode/electrolyte interphase.

2.0 THE Pd+D CODEPOSITION PROCESS.

The codeposition process is a process of palladium electrodeposition from a Pd^{2+} salt solution onto a substrate which does not absorb deuterium, *eg*, Au or Cu [2]. The applied cell current or potential are adjusted to deposit the Pd film in the presence of evolving deuterium. The advantage offered by the codeposition process rests with the morphology of the Pd electrode. The Pd electrode exhibits a "carpet-like" appearance, *ie*, the structure that assures locally a non-uniform distribution of current density and/or overpotentials as well as a very rapid and high absorption of deuterium [3]. Simultaneous evolution of gas bubbles introduces an additional component, namely, a source of random distribution of localized gradients (electrical, mechanical and chemical).

[1] Naval Command, Control and Ocean Surveillance Center, RDT & E Division, San Diego, CA. Author to whom correspondence should be addressed: E-mail address bossp@nosc.mil

3.0 RESULTS

The effectiveness of the codeposition technique with regard to the generation of nuclear and thermal events was demonstrated during the initial phase of our investigation [2]. Early results confirmed excess enthalpy production and X-ray emission. The excess enthalpy was deduced from the temperature difference, namely, higher temperatures were measured on the working electrode than in the electrolyte. The X-ray emanation was recorded on a photographic film placed in close proximity to the Pd electrode. Also, the concentration of tritium in the electrolyte phase was found to be substantially higher than expected from the known value of the separation factor.

These qualitative results were questioned on grounds of not being realistic. Typically, radiographs were not considered to be proof of electromagnetic radiation because they might result from mechanical or chemical interactions. Higher temperatures of the Pd electrode were attributed to the presence of a resistive film rather than a heat source. To prevent such criticisms, we developed a quantitative treatment which we present here in the following order: tritium generation rates, X-ray spectra and the thermal events associated with the Pd+D codeposition.

3.1 Tritium generation rates.

Details of the experimental arrangement, analytical procedure and modeling are given in [3]. Here, only essential points are presented in the condensed form.

3.1.1 Experimental arrangement and error analysis. Experimental arrangement and the sampling profile are shown in Fig. 1a and Fig. 1b. The electrolysis was under galvanostatic control and the sampling routine allowed for the accurate determination of the electrolyte volume and composition at the beginning and end of each time period. Error analysis involved the assessment of the precision of measurements in electrolyte volume, sampling/addition time intervals, constancy of cell current and tritium analysis. The typical error of ± 1.2 dpm (in Fig. 2 and Fig. 3) is not the statistical error of counting but the cumulative uncertainty due to the propagation of errors as determined by procedure commonly used in the treatment of experimental data.

3.1.2 Modeling. In a closed system, the concentration of deuterium in the electrolyte phase is computed by solving Eqs. (1) and (2)

$$d(fm)/dt = \Sigma f_n r_n + q \tag{1}$$

$$dm/dt = \Sigma r_n \tag{2}$$

where f is the tritium mass fraction, m denotes the mass of electrolyte, r is the rate of mass change and q denotes the rate of tritium produced during the electrolysis and subsequently transferred out of the Pd electrode. The subscript n identifies the relevant process.

The solution of Eqs. (1) and (2) for an open system with $r_1 = 0$, $r_2 = 0$ and constant q over the time interval Δt, is

$$\frac{f(t)}{f(0)} = \left[\frac{m(0) - r(i)\Delta t}{m(0)}\right]^{s-1} + \frac{q}{f(0)(s-1)r(i)}\left\{1 - \left[\frac{m(0) - r(i)\Delta t}{m(0)}\right]^{s-1}\right\} \tag{3}$$

where s is the isotopic separation factor defined here as the T/D atomic ratio.

3.1.3 Tritium distribution. Tritium generation rates are estimated by curve fitting technique or by computer modeling in which an arbitrarily selected q-value is inserted into experimental data and computer matched to obtain agreement with the observed distribution throughout the duration of the experiment. The essential difference between the method employed here and elsewhere is in the determination of the numerical value of the separation factor, s. This number is usually taken from the literature and may, or may not, represent the kinetic and thermodynamic properties of the interphase pertinent to the experimental conditions. Here, the value of the separation factor is determined for each experimental run by selecting that value which best fits the recorded data.

Examples of tritium production and distribution paths are illustrated in Fig. 2 and Fig. 3. In particular, Fig. 2a shows two active periods (4/21 - 5/3 and 5/19 - 5/21) separated by two weeks of inactivity. The computed (solid circles) and experimental points (open circles) for the indicated sampling and current profile, suggest that tritium produced in the course of electrolysis, first entered the liquid phase with its distribution governed by the electrodic reaction with s = 0.68. By inserting in Eq. (3) the following production rates: $q_1 = 4 \times 10^3$, $q_2 = 3 \times 1O^3$, $q_3 = 3 \times 10^3$, and $q_4 = 7 \times 10^3$ atoms/second, an excellent agreement between calculated and observed (experimental) points is obtained., Fig. 2b.

A quite different path is illustrated in Fig. 3, where the tritium distribution favors the gas phase, *ie.* where the distribution is not governed by the electrodic reaction. A direct transfer to the gas phase suggests an intense reaction occurring within the subsurface layer(s) with tritium desorption followed by recombination of D_{ads}. The basis for this conclusion is the enrichment of the liquid phase only, *i.e.*, it follows the calculated concentration by Eq. (3) with the separation factor s = 0.67.

3.2 Detection of soft X - rays.

The radiograph obtained early in the investigation [2] suggested the presence of a weak source of the electromagnetic radiation, most likely soft X-rays. In support of this interpretation as well as to provide additional information, we employed two detectors operating simultaneously, *viz.*, the Si(Li) for the X-rays and the Ge for (rays. The background radiation was continuously monitored by the NaI(TI) detector.

3.2.1 Experimental procedure. The experimental program consisted of three tasks: (i) the assessment of the background radiation over the period of several months, (ii) design of an experimental procedure capable of detection low level radiation and (iii) computer simulation. The detailed description can be found in [5].

3.2.2. Presentation of data. The overview of the radiation intensity (count rate) recorded by the Ge detector (spectral region: 15 - 3000 keV) during the D_2O electrolysis on Pd electrodes with two vastly different surface morphologies is presented in Figs. 4a and 4b for the "carpet-like" and smooth surfaces, respectively. It is seen that the count rate is somewhat higher on "carpet-like" surfaces. More interesting, however, are the initiation times. In the first case, no initiation time was required; in contrast, a few days of electrolysis were needed to observe the same effect on smooth surfaces.

Further confirming evidence of electromagnetic radiation is provided in Fig. 5 where two independently operated detectors simultaneously recorded statistically significant increases in radiation (see section labeled II). It is noteworthy that the external field (high overpotentials) is instrumental in producing higher density of events that generate the X-ray emission.

The X-ray intensity data show a remarkable similarity to the tritium production. In both cases, surface morphology dominates the behavior. In particular, on "carpet-like" surfaces reactions are immediate while longer times are required on smooth surfaces.

3.2.3 Spectrum synthesis/modeling. The X-ray data presented in Fig. 6 were interpreted as resulting from the superposition of weak peaks upon a featureless background, e.g., the sharp peak of Pd K" superimposed upon the bremmstrahlung arising from the oscillating plasma of the cathodically polarized Pd/D system. In support of this conclusion, we created a synthetic spectrum, Fig. 7, consisting of the featureless spectrum of thorium oxide and added to it the X-ray spectrum of americium. The resulting composite is similar in appearance to that recorded, i.e., being consistent with the experimental spectrum.

3.3 Thermal events

An almost immediate occurrence of nuclear events in the course of codeposition (tritium production, X-ray emission) suggests a much simpler approach to the accurate determination of excess enthalpy production. Short initiation times indicate that the calorimeter with quasi-adiabatic walls might be suitable.

3.3.1 Cell/calorimeter modeling. The development of governing equations for an operating electrochemical cell employs the conservation laws (energy and mass) and adjusts the applicable walls and constraints in a manner that is consistent with the cell-design relevant experimental procedure [7]. Applying the conservation of energy (in the enthalpy representation), the time rate of the temperature change after its activation is

$$C^{(1)}dT^{(1)}/dt = Q^{(1)} - j_q^{(1\delta 2)} - J_q^{(1\delta e)} \tag{4}$$

$$C^{(2)}dT^{(2)}/dt = Q^{(2)} - J_q^{(2\delta 1)}J_q^{(2\delta e)} \tag{5}$$

where $C^{(1)}$ and $C^{(2)}$ are heat capacities of the electrolyte and bath, respectively; $Q^{(1)}$ denotes the time rate of heat generated in the electrolyte while $Q^{(2)}$ is the rate st which the heat is supplied to the bath in order to maintain equality of the temperature in the cell and the bath; the J_q's are the heat fluxes exchanged between the electrolyte, bath and environment. Employing for the thermal flux an expression of the form $J_q = k\,)\,T$ and introducing new variables $)\,T = T^{(1)} - T^{(2)}$ and $2 = T^{(1)} - T^{(e)}$, after some manipulation combined with a reasonable assumption, (e.g., low $Q^{(1)}$) , we obtain an equation of the form:

$$\frac{d\Delta T}{a - b\Delta T} = dt \tag{6}$$

which, upon solution, yields information concerning best experimental design and procedure.

3.3.2 Survey of thermal events. An example of the excess enthalpy production within the polarized Pd/D system is shown in Fig. 8, where the excess enthalpy, $0.239C^{(1)})\,T^{(1)} - I_{)t}I(E_c - , E_h)dt$ (y-axis) is plotted against the enthalpy input, $I_{)t}IE_c dt$ (x-axis). In the absence of excess enthalpy production all points would fall on the x-axis while excess enthalpy places these points above the x-axis. Inspection of Fig. 8 reveals two distinct time intervals. Within the first time interval, the points are located below the x-axis because within this time period the faradaic efficiency is less than that part of the cell current which is used for the reduction of Pd^{2+} ions.

A review of data indicates that the rate of excess enthalpy production is not uniform in time or position. When the electrode surface is viewed with an infra red camera [8], we notice a chaotic appearance and disappearance of hot spots which subsequently merge to form larger oscillating islands. **These spots indicate intense, localized heat sources acting for very brief periods of time.**

4.0 Discussion.

While the excess enthalpy production was attributed to nuclear reactions, the direct evidence for nuclear activities was provided by tritium production and further supported by radiation of soft X-rays. The lack of data for two

or more signatures of nuclear activities, simultaneously collected under rigorously controlled experimental conditions, is the weakest link.

A review of observations made during, and following, the codeposition process, show a common thread, namely, unpredictable (with regard to time and position) initiation, uncontrolled periods of activity, and a common response to additives, e.g., Be^{2+} or Mg^{2+} ions. However, the most unusual behavior was noted when the polarized Pd electrode surface was viewed with an infra red camera. These observations point clearly to the importance of the dynamics of the interphase region and its role associated with the transport of deuterium from the adsorbed to absorbed state. In our discussion we examine the proposed models of the inter-phase, the nature of the driving force, and the possible interplay between the various species or their energetic states.

4.1 The interphase.

The interphase region is a layer separating two homogeneous phases: the metallic electrode and liquid electrolyte. For the thermodynamic consistency this layer is viewed as a non-autonomous phase [8]. The solution side of the interphase is well understood, the metallic part has only recently been subjected to comprehensive examination. In particular, the effect of catalytic poisons on the H-population of the interphase was examined with the emphasis on the hydrogen evolution reaction rather than on the interfacial transport. A number of models have been proposed [8-14]. All contain a common feature, namely the accumulation of hydrogen in the subsurface layer. Experimental evidence, e.g., immediate formation of the ß - phase indicates rapid absorption [15]. The entrance of hydrogen into the subsurface layer is associated with swelling resulting in a "modular-like" structure [12].

4.2 Driving forces.

A model that shows a qualitative agreement with experimental data was constructed [15]. This model predicts small asymmetry in loading and unloading; it does not, however, account for changes as large as actually observed [16]. Natural forces driving the deuterium evolution reaction as well as the transport into the Pd electrode interior is the chemical potential, $\mu = \frac{\partial U}{\partial n} | s,v$. The chemical potential of the adsorbed hydrogen and its role with regard to the hydrogen evolution reaction was recently discussed by Jerkiewicz et. al., [13,14] and that of dissolved hydrogen by Wagner [17] with further extension to include high hydrogen content, by Brodowsky [18]. It is the chemical potential of species populating the interphase that is of interest in formulating the "performance envelope." However, the difficulty is in the specification of the internal energy as a function of position within the interphase formed between the polarized Pd electrode with high D content and the electrolyte.

A more realistic model incorporating an active interphase is needed. An approach currently under considerations in this laboratory, is to examine the nature of the driving forces operating in the course of charging/discharging of the polarized Pd electrode.

4.3 Thermal instabilities.

Thermal events occurring during the electrochemical compression of the Pd/D system were, and are, discussed in terms of excess enthalpy produced over a period of time, often several days. Thus, they represent an average value and provide no information on the distribution of heat sources. **However, if the surface of the polarized Pd electrode is viewed with an infra-red camera, it reveals the presence of randomly distributed (in time and space) heat sources of short duration**. This observation is consistent with ideas advanced recently by Fleischmann et. al. [19], that of expressing the heat generation in terms of a number of time dependent variables, Q = f[E(t), 2(t), ...X(t)]. Some of these variables can be controlled by an experimenter, others cannot ("hidden

variables"). Because these variables are interconnected, they can lead to the development of instabilities which, in turn, may or may not be modified by imposing feed-back controls. A much simpler picture can be presented if (i) events take place within the interphase (*ie* subsurface layers), (ii) that the interphase is a non-autonomous phase and (iii) that the adsorbed deuterium travels across the interphase. This is the direction that we contemplate at this time.

5.0 Concluding remarks

An alternate method for the examination of the Fleischmann-Pons effect is the use of the codeposition technique. Employing this method for the electrochemical compression of the Pd/D system, we established as follows:

(I) Emission of soft X-rays.

(ii) Tritium production at rates ranging from 10^3 to 10^4 atoms per second.

(iii) Excess enthalpy production with random distribution of reaction sites.

REFERENCES

1. C. Bartomoleo, M. Fleischmann, G. Larramona, S. Pons and J. Roulette, "Alfred Coehn and After: The " ß (of the Palladium-Hydrogen System," *Fusion Technology*, vol 26, no 4T, Proceedings of ICCF 4, p 23 (1995).
2. S. Szpak, P.A. Mosier-Boss and J.J. Smith, *J. Electroanal. Chem.*., vol 302, p 255 (1991).
3. S. Szpak, P.A. Mosier-Boss and J.J. Smith, *J. Electroanal. Chem.*, vol 379, p 121 (1994).
4. S. Szpak, P.A. Mosier-Boss, R.D, Boss and J.J. Smith, *J. Electroanal. Chem*., vol 373, p 1 (1994).
5. S. Szpak and P.A. Mosier-Boss, *Physics Letters A*, vol 210, p 382 (1996).
6. S. Szpak and P.A. Mosier-Boss, *Physics Letters A*, in press.
7. S. Szpak and P.A. Mosier-Boss, *J. Phys. Chem.*. submitted.
8. R. Delay, I. Prigogine and A. Bellemans, Surface Tension and Adsorption, Chapters XX and XXI, Longmans and Green, London (1966).
9. R.J. Behm, V. Penka, M-G Kattania, K. Christmann and G. Ertl, *J. Chem. Physics*, vol 78, p 7486 (1983).
10. R.V. Bucur and F. Bota, *Electrochim. Acta*, vol 28, p 1373 (1983).
11. R.V. Bucur and F. Bota. *Electrochim. Acta*, vol 29, p 103 (1984).
12. T. Ohmori, K. Sakamaki, K. Hashimoto and A. Fujishina, *Chemistry Letters* (Japan) (1991).
13. G. Jerkiewicz and A. Zolfaghari, *J. Electrochem. Soc.*, vol 143, p 1240 (1996).
14. G. Jerkiewicz, J.J. Brodzinski, W. Chrzanowski and B.E. Conway, *ibid.*, vol 142, p 3755 (1995)
15. S. Szpak, P.A. Mosier-Boss, C.J. Gabriel and J.J. Smith, *J. Electroanal. Chem.*, vol 365, p 275 (1994)
16. A.M. Riley, J.D. Seader, D.W. Pershing and C. Walling, *J. Electrochem. Soc.*, vol 139, p 1342 (1992)
17. C. Wagner, *J. Phys. Chem., A*, vol 193, p 386 (1944)
18. H. Brodowsky, *Ber. Bunsenges. Phys. Chem.*, vol 76, p 797 (1972)
19. M. Fleischmann, S. Pons, M. LeRoux and J. Roulette, "Calorimetry of the PD-D_2O System: The Search for Simplicity and Accuracy ," *Fusion Technology*, vol 26, no 4T, ICCF4, p 323 (1994)

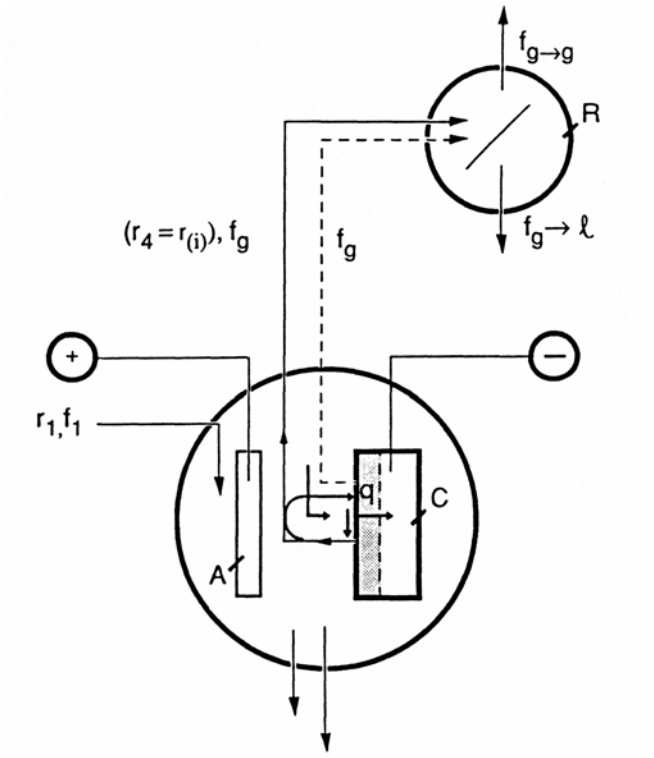

Fig. 1a – Mass balance on electrolyte: r, rates of mass change (subscripts 1, 2, 3 and 4 indicate electrolyte addition, removal by sampling, evaporation and electrolysis respectively); f, tritium mass fraction (subscripts g and l denote gas and liquid phases).

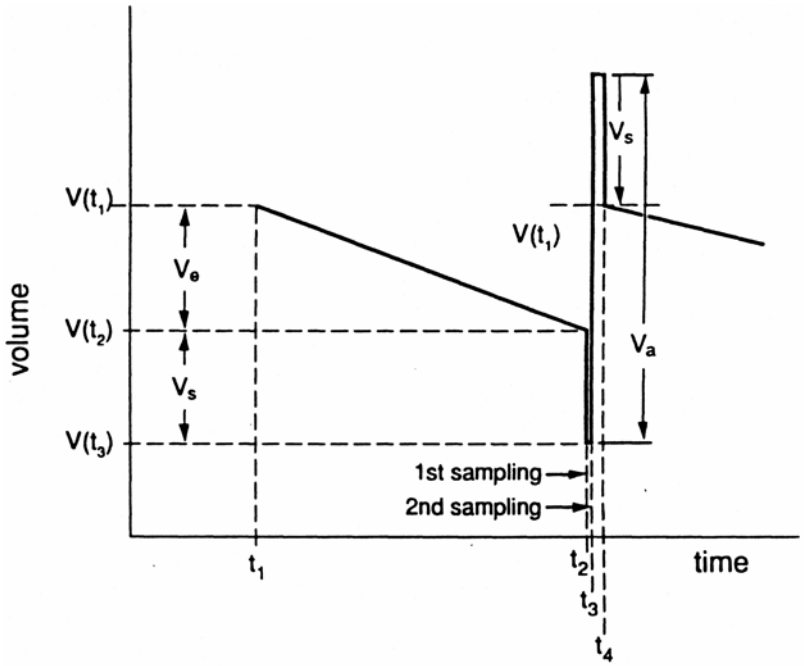

Fig. 1b – Sampling procedure for tritium generation in open cells: V_e is the volume lost by electrolysis; V_s is the sampling volume; V_a is the electrolyte volume added to restore prior conditions.

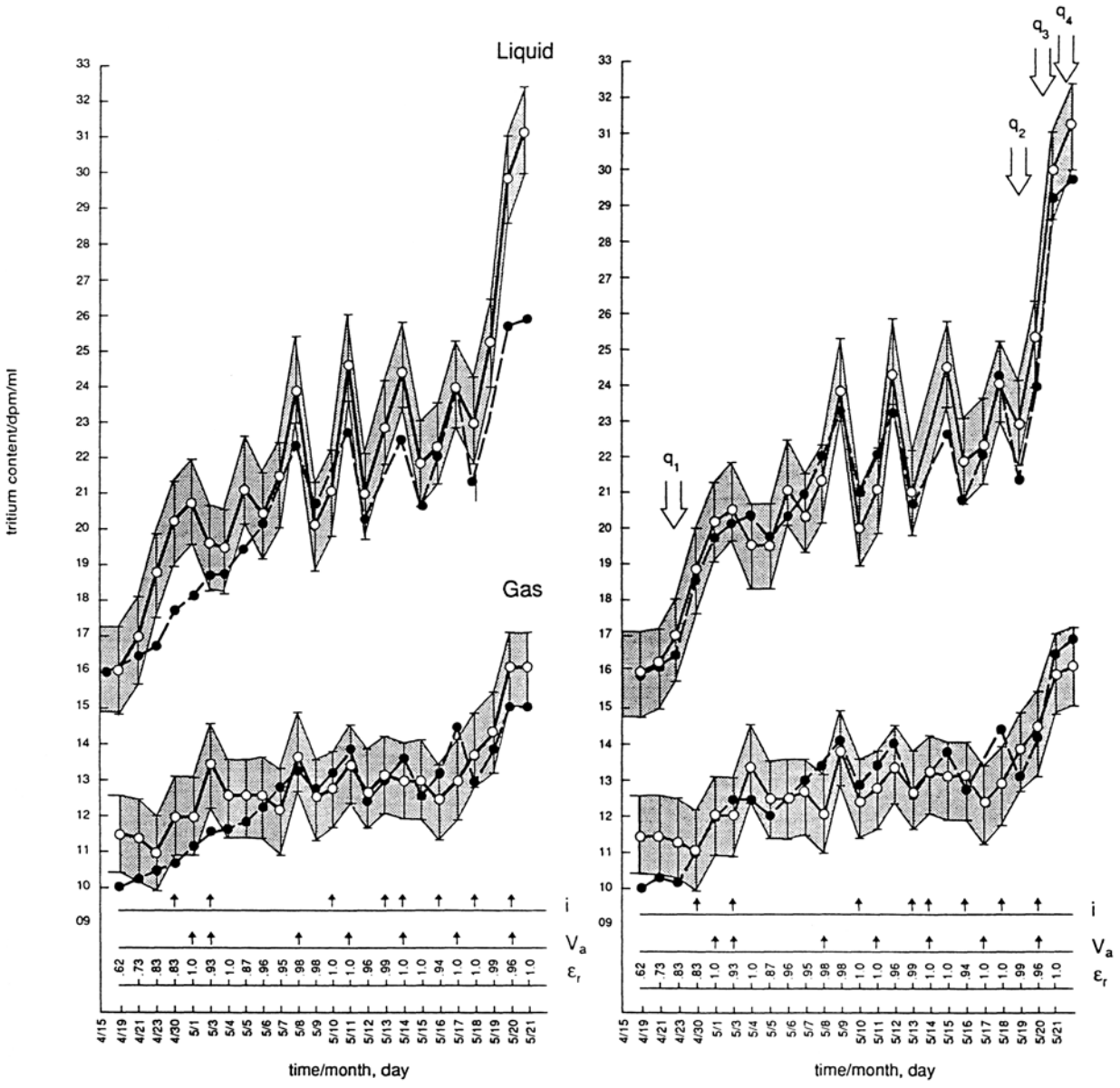

Fig. 2 – Tritium two-phase distribution. Electrode – Pd deposited from $Pd(NH_3)_2Cl_2$; Electrolyte – 0.3 M Li_2SO_4 a: recorded data; b: computer matched.

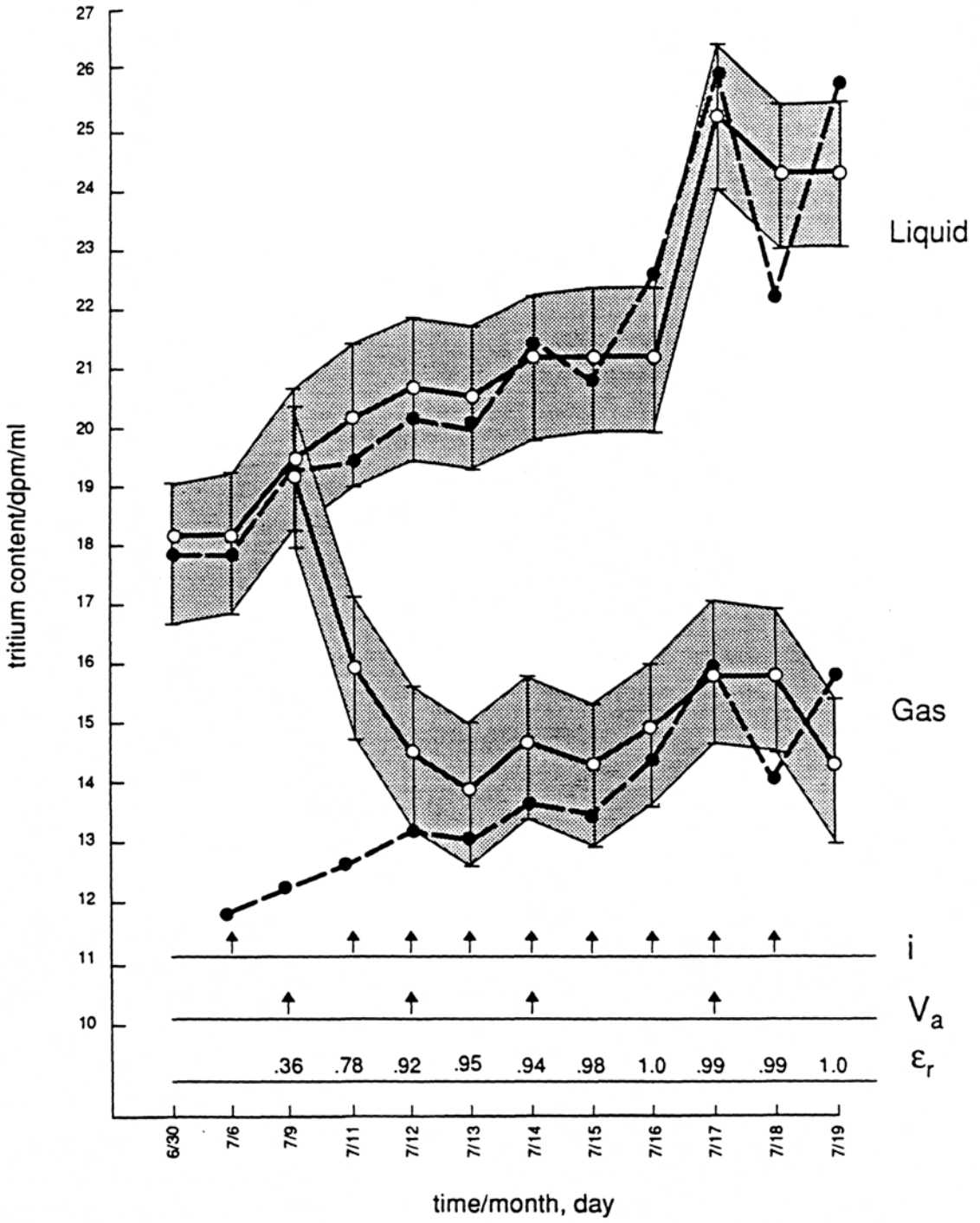

Fig. 3 – Tritium two-phase distribution during and after codeposition. Electrolyte – 0.6 LiCl

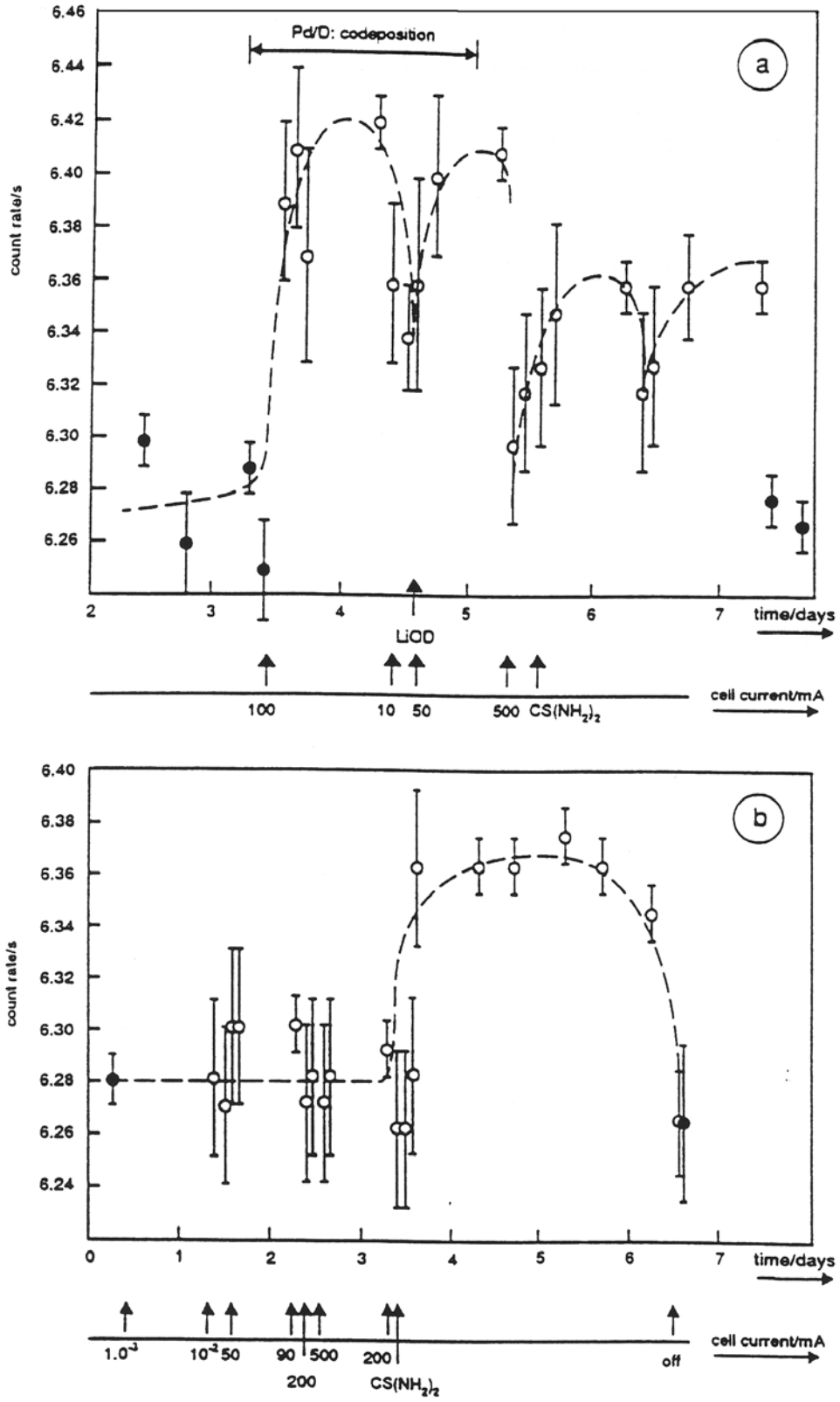

Fig. 4 - Electromagnetic flux emitted during cathodic polarization of the Pd/D system: Spectral region 15 - 3000 keV (indicated are cell current profile and additives): background - solid circles; operating cell - open circles.

Fig. 4a - Electrolyte - 0.003 M $PdCl_2$ - 0.3 M LiCi - D_2O; LiOD added after depletion of Pd^{2+} ions.

Fig. 4b - Electrolyte - 0.1 M LiOD.

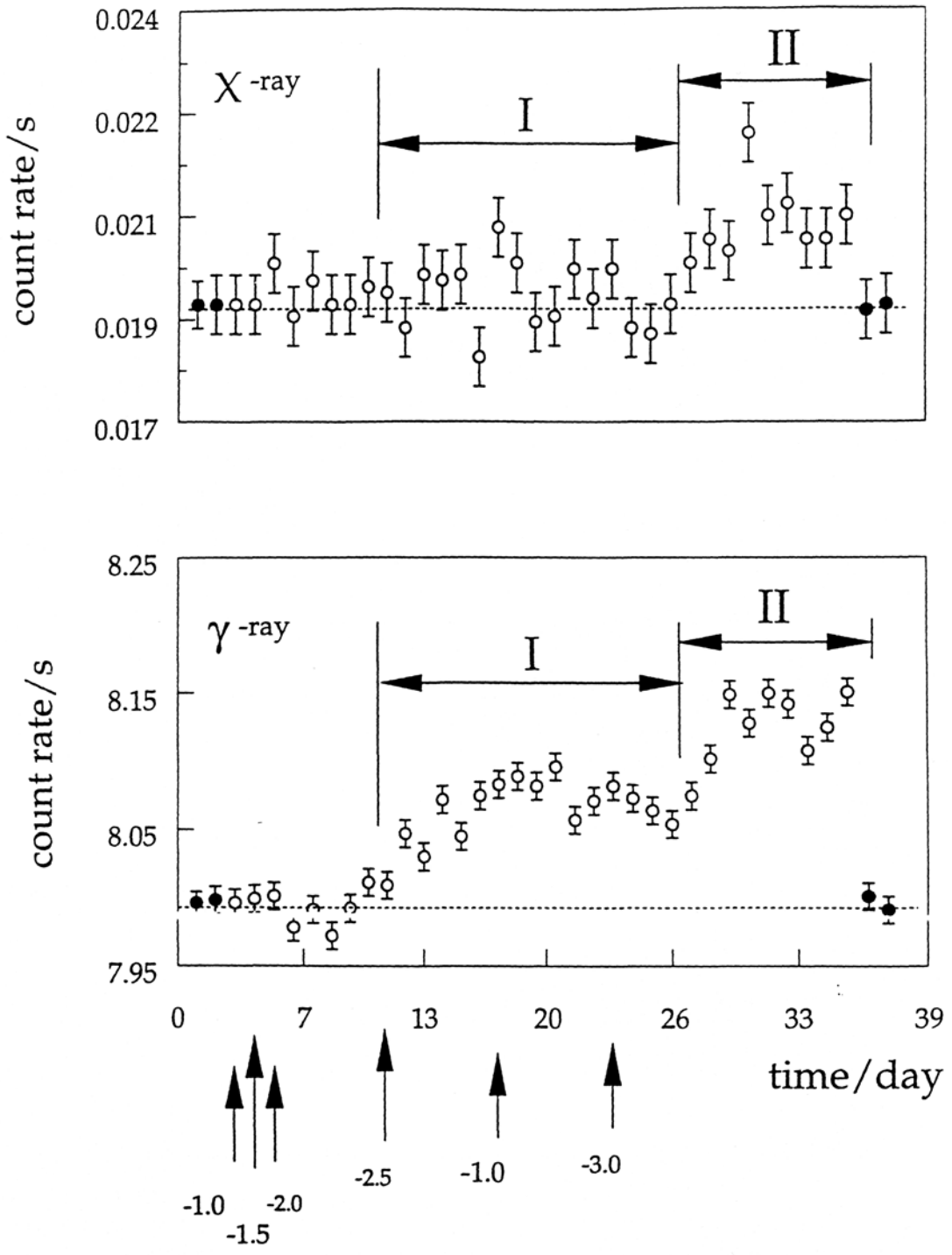

Fig. 5 - Electromagnetic flux emitted during cathodic polarization of the Pd/D system, upper - spectral region 7-40 keV; lower - spectral region 40 - 300 keV. Arrows indicate the applied overpotential (vs Ag/AgCl reference); background - solid circles: operating cell - open circles.

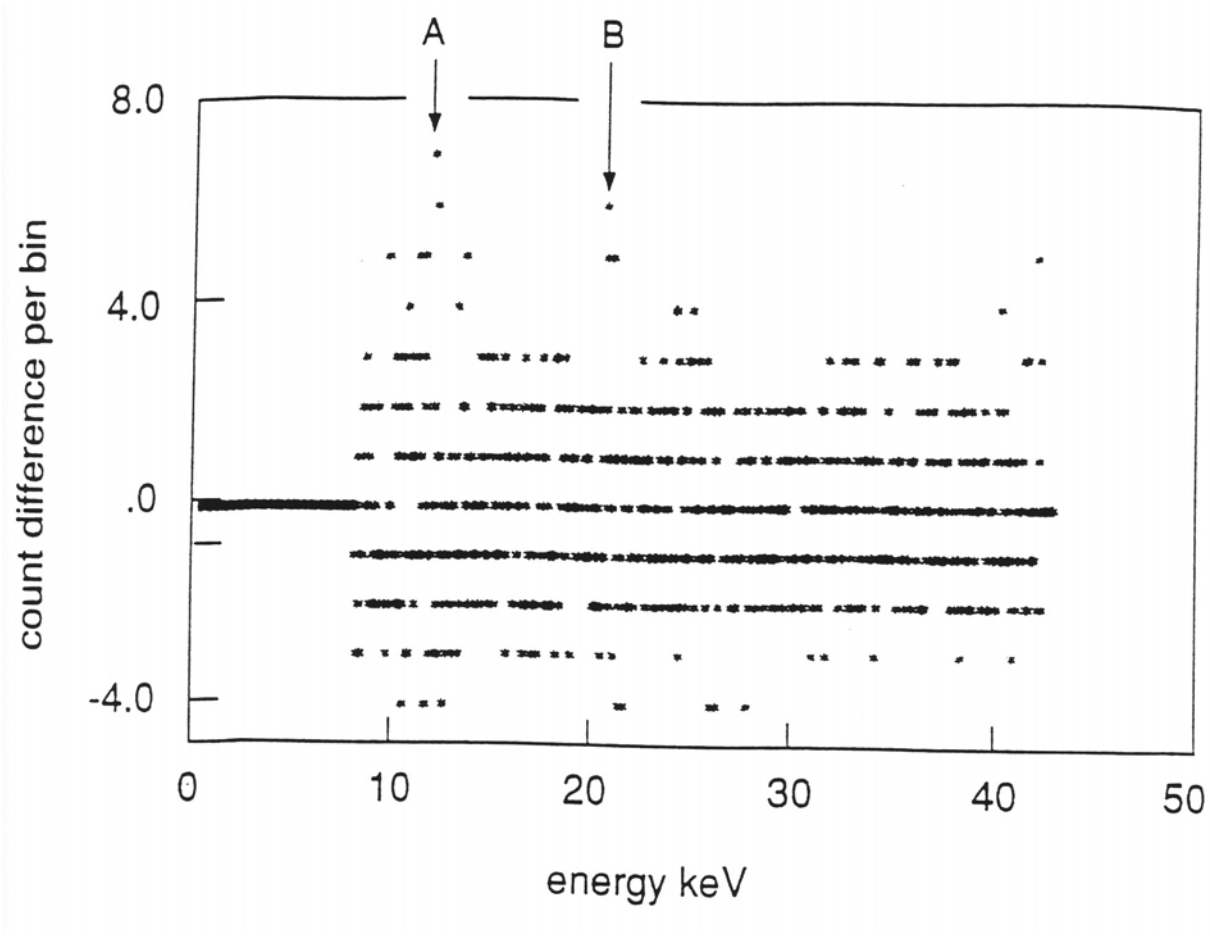

Fig. 6 - X-ray spectrum emitted during cathodic polarization of the Pd/D system. Spectral region 7-40 keV; background spectrum subtracted.

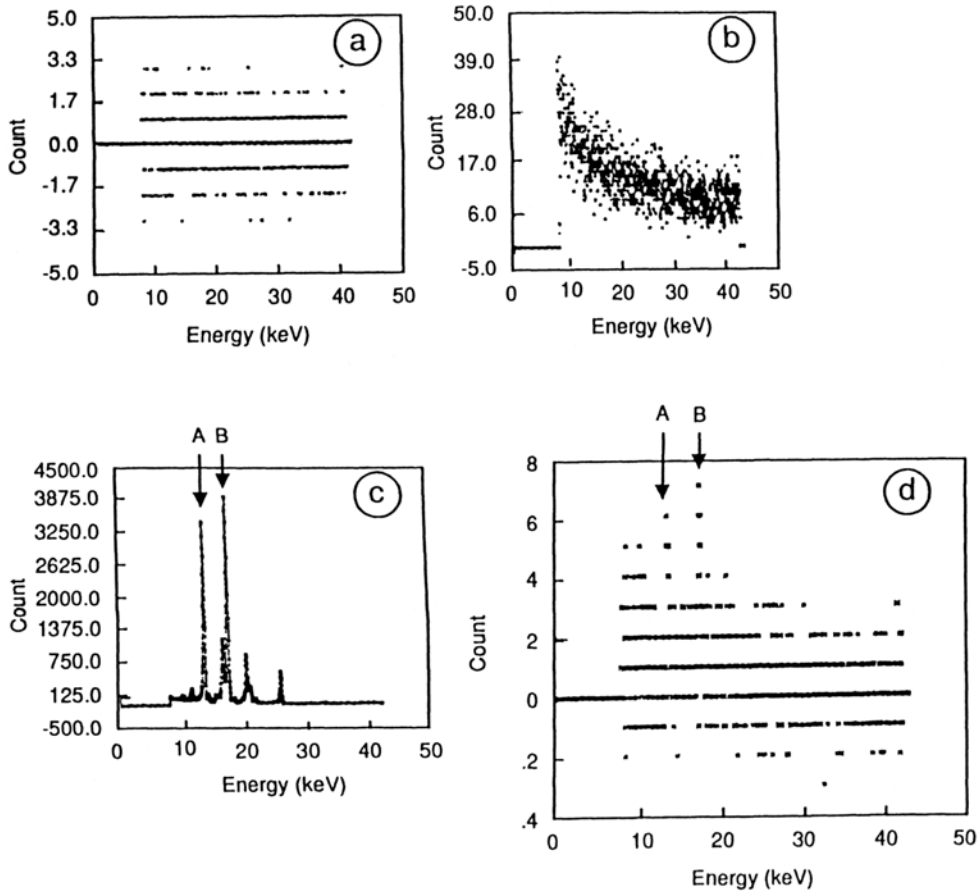

Fig. 7 - Computer simulation of the addition (superposition) of weak spectral lines to the broad distribution.

a - The difference of two background files (symmetric distribution about zero);
b - Energy distribution of the X -ray emanating from thorium oxide;
c - X-ray spectrum of americium;
d - Computer simulated energy distribution for a sum of 0.0015 Am spectrum and 0.02 ThO - 2 spectrum and a difference of two separate backgrounds, all normalized to a 24 hr period.

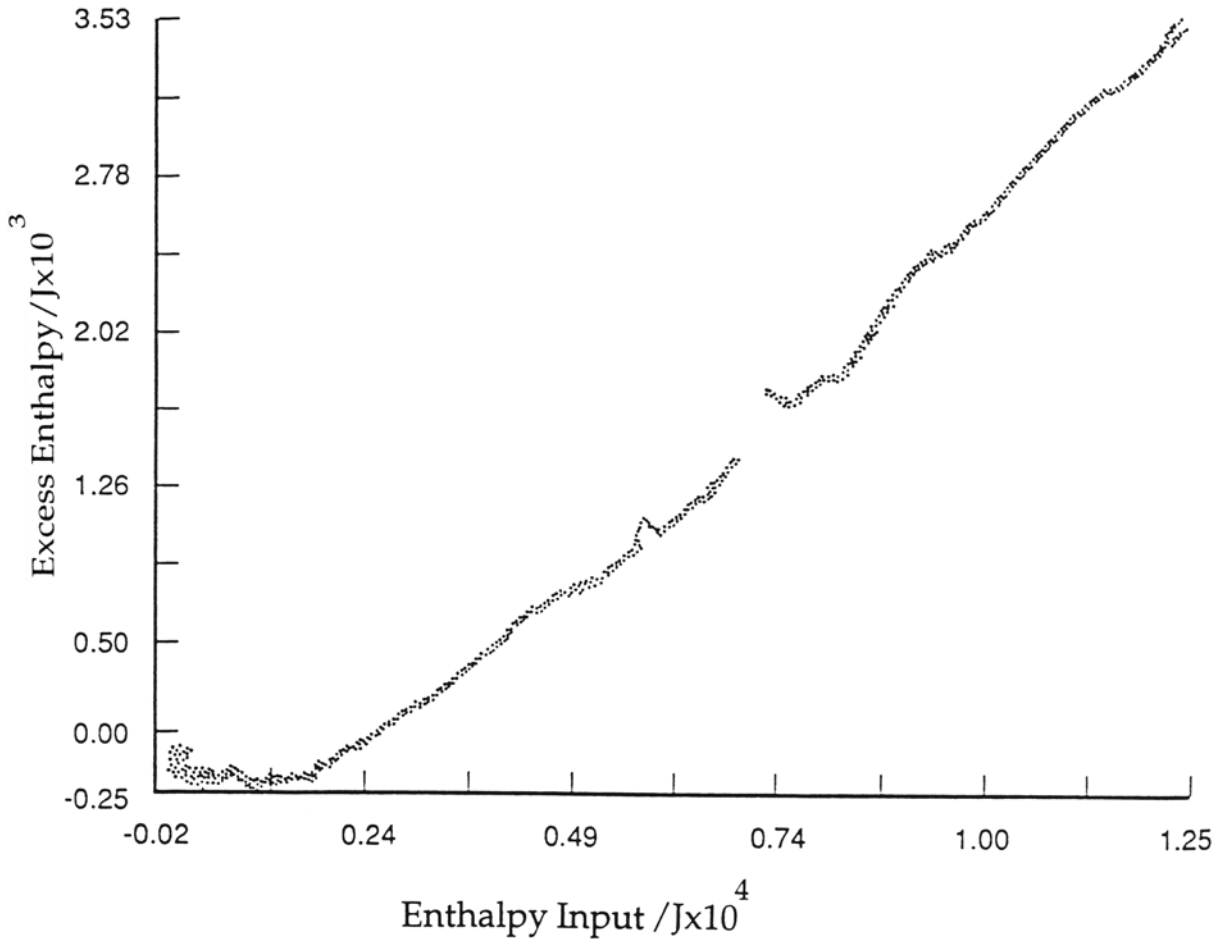

Fig. 8. Excess enthalpy generated in the course of codeposition.